nature communications



Article

https://doi.org/10.1038/s41467-024-52033-x

Phosphorylation activates master growth regulator DELLA by promoting histone H2A binding at chromatin in *Arabidopsis*

Received: 17 October 2023

Accepted: 22 August 2024

Published online: 03 September 2024



Xu Huang $\textcircled{0}^{1,7}$, Rodolfo Zentella $\textcircled{0}^{1,4,5,7}$, Jeongmoo Park 1,6,7 , Larry Reser 2 , Dina L. Bai 2 , Mark M. Ross $\textcircled{0}^2$, Jeffrey Shabanowitz $\textcircled{0}^2$, Donald F. Hunt $\textcircled{0}^{2,3}$ & Tai-ping Sun $\textcircled{0}^1$

DELLA proteins are conserved master growth regulators that play a central role in controlling plant development in response to internal and environmental cues. DELLAs function as transcription regulators, which are recruited to target promoters by binding to transcription factors (TFs) and histone H2A via their GRAS domain. Recent studies showed that DELLA stability is regulated post-translationally via two mechanisms, phytohormone gibberellin-induced polyubiquitination for its rapid degradation, and Small Ubiquitin-like Modifier (SUMO)-conjugation to increase its accumulation. Moreover, DELLA activity is dynamically modulated by two distinct glycosylations: DELLA-TF interactions are enhanced by O-fucosylation, but inhibited by O-linked N-acetylglucosamine (O-GlcNAc) modification. However, the role of DELLA phosphorylation remains unclear as previous studies showing conflicting results ranging from findings that suggest phosphorylation promotes or reduces DELLA degradation to others indicating it has no effect on its stability. Here, we identify phosphorylation sites in REPRESSOR OF gal-3 (RGA, an AtDELLA) purified from *Arabidopsis* by mass spectrometry analysis, and show that phosphorylation of two RGA peptides in the PolyS and PolyS/T regions enhances RGA activity by promoting H2A binding and RGA association with target promoters. Notably, phosphorylation does not affect RGA-TF interactions or RGA stability. Our study has uncovered a molecular mechanism of phosphorylation-induced DELLA activity.

The phytohormone gibberellin (GA) plays a pivotal role in regulating plant growth and development, from promoting seed germination, vegetative growth to floral induction and flower and fruit development¹. GA activates its signaling pathway by binding to its receptor GIBBERELLIN INSENSITIVE1 (GID1)². This interaction triggers

the degradation of DELLA proteins, which are repressors in the GA-signaling pathway, through the ubiquitin-proteasome pathway³. Specifically, GA-GID1 induces the polyubiquitination of DELLAs, a process facilitated by F-box proteins—GID2 in rice (*Oryza sativa*) and SLEEPY1 (SLY1) in *Arabidopsis*. These F-box proteins are key components of the

¹Department of Biology, Duke University, Durham, NC 27708, USA. ²Department of Chemistry, University of Virginia, Charlottesville, VA 22904, USA. ³Department of Pathology, University of Virginia, Charlottesville, VA 22903, USA. ⁴Present address: U.S. Department of Agriculture, Agricultural Research Service, Plant Science Research Unit, Raleigh, NC 27607, USA. ⁵Present address: Department of Crop and Soil Sciences, North Carolina State University, Raleigh, NC 27695, USA. ⁶Present address: Syngenta, Research Triangle Park, NC 27709, USA. ⁷These authors contributed equally: Xu Huang, Rodolfo Zentella, Jeongmoo Park. ⋈ e-mail: tps@duke.edu

SCF (Skp1-Cullin-F-box protein) E3 ubiquitin ligase complex^{4,5}. DEL-LAs are nuclear-localized transcription regulators found in all land plants⁶. Further studies show that DELLA orthologs are conserved master growth regulators, which play a central role in coordinating multiple signaling activities in response to biotic and abiotic cues^{3,7} DELLAs belong to a subfamily of plant-specific transcription regulators known as GRAS (for GAI, RGA, and SCARECROW). All GRAS family members share a conserved C-terminal GRAS domain, while the DELLA subfamily also contains a unique N-terminal DELLA domain, characterized by the DELLA sequence motif¹⁰⁻¹³. The DELLA domain is required for GA-induced degradation. It interacts with the GA-bound receptor GID1, thereby promoting recruitment of the SCF^{SLY1/GID2} E3 ubiquitin ligase for polyubiquitination and proteolysis of the DELLA protein by the 26S proteasome^{2,4,5,14-18}. DELLAs mediate transcription reprogramming by direct interaction of their GRAS domain with hundreds of transcription factors (TFs)^{7-9,19,20}. By characterizing new missense alleles of an Arabidopsis DELLA, REPRESSOR OF ga1-3 (RGA), we recently revealed that formation of the TF-RGA-histone H2A complexes at the target chromatin is essential for RGA activity²¹. The GRAS domain consists of five conserved subdomains: Leu Heptad Repeat 1 (LHR1), VHIID, LHR2, PFYRE and SAW, three of which (VHIID, PFYRE and SAW) were named after the conserved amino acid motifs¹⁰. The RGA LHR1 subdomain facilitate its recruitment to target promoters by binding to TFs, while RGA-H2A interaction via the PFYRE subdomain stabilizes the TF-RGA-H2A complex at the target chromatin^{9,21}. In addition, mutant analyses showed that the VHIID and LHR2 subdomains are involved in F-box protein binding²²⁻²⁴.

In addition to GA-dependent proteolysis mediated by polyubiquitination, DELLA activity is also modulated by several other posttranslational modifications (PTMs) including Small Ubiquitin-Like Modifier (SUMO)-conjugation (SUMOylation), glycosylation, and phosphorylation^{25–28}. SUMOylated DELLA under salt-stress conditions was shown to sequester GID1 in a GA-independent manner, consequently increasing the amount of non-SUMO-DELLA and causing growth restriction²⁹. On the other hand, de-SUMOvlation of DELLA under regular growth conditions promotes stamen filament elongation³⁰. Besides SUMOylation, recent genetic and biochemical studies revealed that DELLA activity is oppositely regulated by two distinct types of O-glycosylation of Ser and Thr residues; i.e., O-linked N-acetylglucosamine (O-GlcNAc) and O-fucose modifications^{26,27}. O-fucosylation of DELLA by the protein fucosyltransferase SPINDLY (SPY) enhances DELLA binding to TFs [e.g., BRASSINAZOLE-RESISTANT1 (BZR1) and PHYTOCHROME INTERACTING FACTORS (PIFs)], whereas O-GlcNAcylation of DELLA by the O-GlcNAc transferase SECRET AGENT (SEC) reduces DELLA activity^{31,32}. It was proposed that O-Fuc and O-GlcNAc modifications may modulate DELLA activity and plant growth in response to nutrient availability as O-GlcNAcylation serves as a nutrient sensor in metazoans 32,33.

Besides SUMOylation and O-glycosylation, DELLA proteins are also phosphorylated²⁵. However, the precise role of phosphorylation in DELLA function is unclear as several studies have provided conflicting results. Early studies showed that GA promotes phosphorylation of the rice DELLA, SLENDER RICE1 (SLR1) in the F-box gid2 mutant4, and phosphorylated DELLA proteins preferentially bind to the F-box protein by in vitro pull-down assays^{34,35}. These findings suggest that phosphorylation of DELLA promotes its degradation. However, a subsequent study found that phosphorylation of SLR1 does not affect F-box protein GID2 binding affinity, suggesting that GA-induced SLR1 degradation does not require its phosphorylation³⁶. On the other hand, pharmacological studies in seedlings or in vitro showed that phosphatase inhibitors block DELLA degradation, suggesting that dephosphorylation of DELLAs promotes their proteolysis^{37–39}. Moreover, silencing of TOPP4 encoding a type one phosphatase in Arabidopsis causes increased GFP-RGA accumulation⁴⁰. Another study further showed that phosphorylation of SLR1 by a casein kinase I (CK1), EARLIER FLOWERING1 (EL1), promotes its stability. The el1 mutant flowers early and exhibits elevated GA response⁴¹. Moreover, GAinduced degradation of SLR1-YFP in the el1 mutant background was faster than in the WT background, suggesting that EL1 enhances DELLA stability. However, SLR1 phosphorylation by EL1 was only demonstrated in vitro, and phosphosites in SLR1 have not been identified. The potential role of phosphorylation has also been studied by mutating conserved Ser/Thr residues (to Ala or Asp/Glu) in Arabidopsis DELLAs, RGL2 or RGA and then monitoring the protein stability/activity in tobacco BY2 cells (RGL2) or in transgenic Arabidopsis (RGA)^{38,42}. Six Ala substitutions at T308, T356, T449, S479, T571 and S578 within the GRAS domain of RGA (named RGA6A-GFP) appear to reduce RGA protein stability, whereas Asp mutations (RGA6D) stabilize RGA42. Again, these results suggest that phosphorylation may enhance DELLA stability, although there is no evidence of phosphorylation of these S/T residues in planta. In addition, these Ser/Thr-to-Ala substitutions are located in the GRAS domain and may affect RGA/RGL2 activity directly.

To elucidate the role of phosphorylation in regulating DELLA function, it is crucial to identify DELLA phosphorylation sites in vivo and conduct functional analysis in planta. By affinity purification from plant extracts followed by MS/MS analysis, we have identified several phosphosites in RGA. RGA phosphorylation was elevated under GA-deficient conditions, although phosphorylation does not affect its stability. Importantly, co-IP and ChIP-qPCR assays showed that phosphorylation within the RGA PolyS/T region promotes its interaction with H2A and its association with target promoters, revealing the mechanism of phosphorylation-induced RGA function.

Results

Elevated RGA phosphorylation under GA-deficient conditions

To investigate the role of DELLA phosphorylation, we first examined whether relative phosphorylation levels (vs. unphosphorylated form) of endogenous REPRESSOR OF gal-3 (RGA, an AtDELLA) are affected in different GA mutant backgrounds. We found that relative phospho-RGA (pRGA) levels were elevated under GA-deficient conditions, either in a GA-biosynthesis mutant ga1-13 or WT Col-0 treated with GA biosynthesis inhibitor paclobutrazol (PAC), compared to WT (Fig. 1a). Because phospho-RGA could not be separated clearly from the unphosphorylated form by standard SDS-PAGE, we used Phos-tag SDS-PAGE to detect phospho-RGA as the phosphate binding metal complex in the Phos-tag Acrylamide reagent causes retarded gel mobility of phosphorylated proteins⁴³. To monitor RGA phosphorylation more easily, we also analyzed His-FLAG-RGA in the P_{RGA}:His-FLAG-RGA ga1-13 della pentuple (ga1 dP) transgenic line. Phosphatase treatment confirmed that the slower mobility band is phosphorylated His-FLAG-RGA (Fig. 1b). We further analyzed relative phospho-RGA levels in the F-box protein mutant sly1-10, which is a semi-dwarf with reduced GA responses because DELLAs accumulate to high levels⁵. Due to the feedback mechanism that regulates GA biosynthesis, the sly1 mutant contains elevated amounts of active GAs. The high GA content in sly1 promotes proteolysis-independent attenuation of DELLAs by GID1 binding⁴⁴. This is consistent with the less severe phenotype of the *sly1* mutant compared to ga1, although RGA accumulates to much higher level in sly1 than in ga1 (Fig. 1c, d). Phos-tag gel blot analysis showed that the relative phospho-RGA levels (pRGA vs. unphosphorylated form) in sly1 were notably lower than those in ga1 (Fig. 1d). These results indicate that RGA phosphorylation is elevated under GA deficiency (ga1) and reduced under high bioactive GA content (sly1). GA treatment induced degradation of both phosphorylated and unphosphorylated RGA proteins (Fig. 1e), indicating that phosphorylation does not alter RGA stability.

The reduced RGA phosphorylation by GA resembled the previous finding in rice showing that expression of *EL1* encoding a CK1 protein kinase is downregulated by GA and that *EL1* phosphorylates SLR1 (the rice DELLA protein) in vitro⁴¹. There are four *Arabidopsis* EL1-LIKES

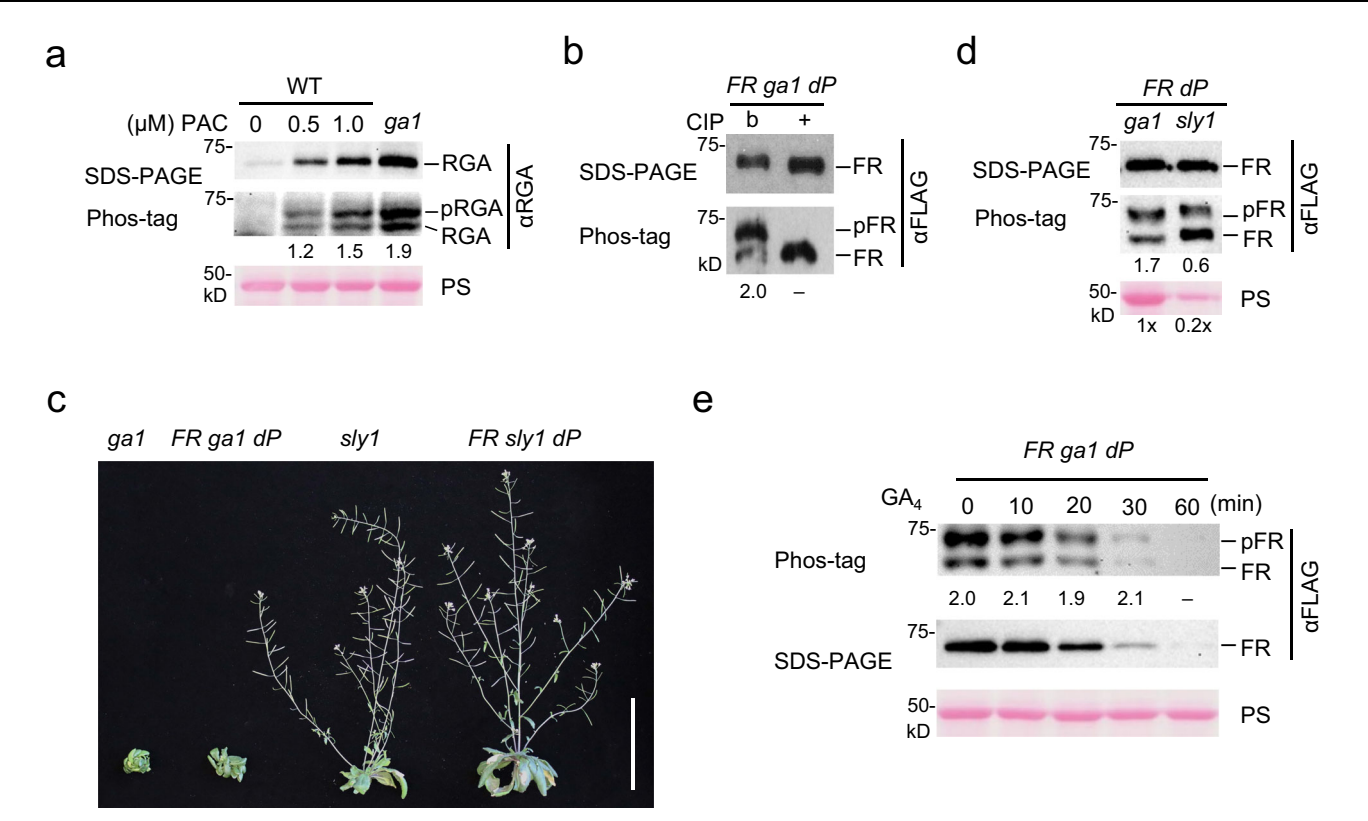


Fig. 1 | **GA deficiency promotes RGA phosphorylation. a** Increased RGA phosphorylation by PAC treatment or *ga1* mutation. WT and *ga1* seedlings grown on media with different concentration of PAC for 10 days under long-day (LD) conditions. **b** RGA phosphorylation pattern with or without CIP (Calf Intestinal Alkaline Phosphatase) treatment. **b** boiled CIP. **c** Representative 42d-old plants as labeled. *FR*, P_{RGA} :*His-FLAG-RGA*. Bar = 3 cm. **d** FLAG-RGA phosphorylation pattern in *FR ga1 dP* and *FR sly1 dP* lines. The blot contained total protein extracted from these lines. The *FR sly1 dP* protein sample was diluted 5-fold compared to that of *FR ga1 dP* because FLAG-RGA accumulated to very high levels in the *sly1* background. **e** RGA phosphorylation did not affect GA-induced degradation. The protein blot

contained total protein from P_{RGA} :His-FLAG-RGA ga1 dP seedlings after $0.1\,\mu\text{M}$ GA₄ treatment for the indicated time. In $\bf a$, $\bf b$, $\bf d$, $\bf e$, proteins were analyzed by both standard SDS-PAGE and Phos-tag gels (containing 25 μ M Phos-tag Acrylamide), followed by immunoblotting with an anti-RGA antibody (in $\bf a$) or anti-FLAG antibody ($\bf b$, $\bf d$, $\bf e$). pRGA, phosphorylated RGA. pFR, phosphorylated His-FLAG-RGA. Ponceau S (PS)-stained blot in $\bf a$, $\bf e$ indicated similar sample loading. The ratios of phosphorylated RGA/unphosphorylated RGA are shown below the Phos-tag gel blots in $\bf a$, $\bf b$, $\bf d$, $\bf e$. -, not detectable. Representative images of 2 biological repeats are shown. Source data are provided in the Source Data file.

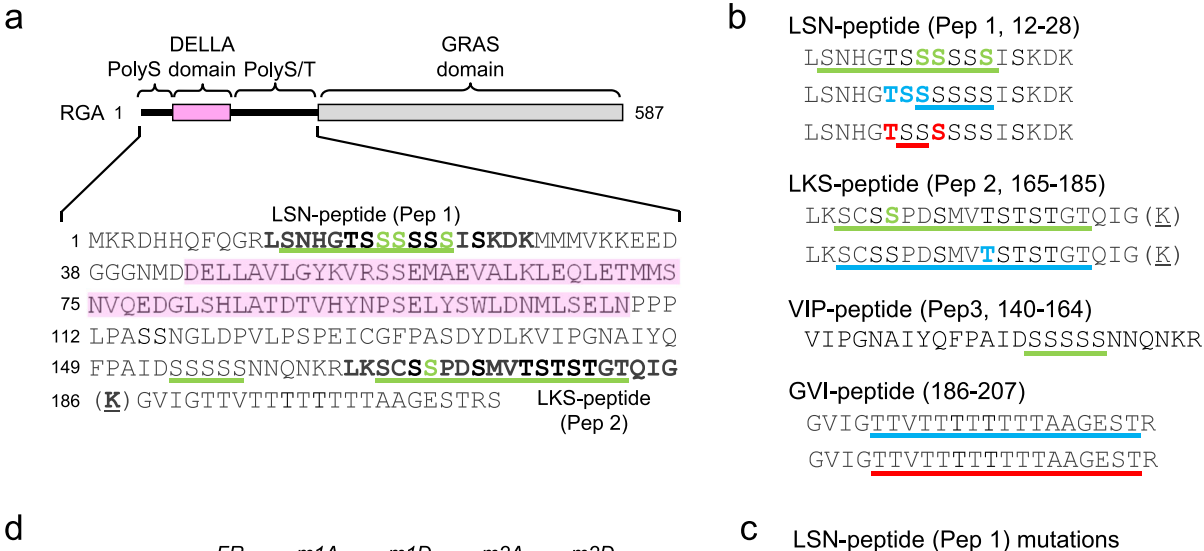
(AEL1-4)⁴⁵, which are also known as MUT9-LIKE KINASEs (MLKs)⁴⁶ and PHOTOREGULATORY PROTEIN KINASEs (PPKs)⁴⁷. To determine whether MLKs phosphorylate RGA in *Arabidopsis*, we introduced P_{RGA} :*His-FLAG-RGA* into double and triple *mlk* mutants. However, our Phos-tag gel analysis did not detect any notable reduction in RGA phosphorylation in these mutants, suggesting that MLK1-4 do not play a major role in RGA phosphorylation (Supplementary Fig. 1).

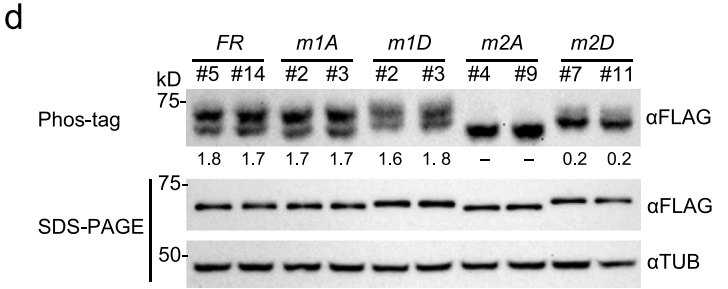
Besides GA levels, DELLA-modulated growth responses can be also affected by several other hormones [e.g., brassinosteroid (BR), salicylic acid (SA), jasmonate (JA), and abscisic acid (ABA)] and by abiotic stresses (e.g., osmotic and salt stresses)³. However, we did not detect notable changes in RGA phosphorylation by these treatments (Supplementary Fig. 2).

Identification of RGA phosphorylation sites by LC-ESI-MS/MS

To identify phosphosites in RGA by MS analysis, we used transgenic *Arabidopsis* carrying P_{RGA} :*His-FLAG-RGA*^{GKG} in either *ga1-3 rga-24* or *sly1-10 rga-24* backgrounds. His-FLAG-RGA^{GKG} contains an extra trypsin cleavage site by inserting a Lys (K) residue within the PolyS/T region that enables MS detection of this region³¹ (Fig. 2a). His-FLAG-RGA^{GKG} is functional in planta to rescue the *rga* null phenotype³¹. The affinity-purified His-FLAG-RGA^{GKG} samples from *ga1-3 rga-24* and *sly1-10 rga-24* backgrounds were analyzed by online liquid chromatography-electrospray ionization-tandem mass spectrometry (LC-ESI-MS/MS). Semi-quantitative analysis for relative peptide abundances was determined from ion currents detected in the MS1 survey scans. It should be

noted that less than 2-fold differences by this analysis may not be considered significant. Two highly phosphorylated RGA peptides, LSNpeptide [LSNHGTSSSSSISK(DK), 30.5%] and LKS-peptide [(LK) SCSSPDSMVTSTSTGTQIGK, 28.6%], were identified in RGAGKG purified from the ga1 background (Fig. 2a, b, Table 1, Supplementary Table 1, and Supplementary Data 1-5). Low levels of phosphorylation (2.5%) were also detected in another RGA peptide (VIP-peptide, VIPG-NAIYQFPAIDSSSSNNQNKR) that is immediate upstream of LKSpeptide. To distinguish among these three peptides more easily, we will designate them as Pep1 (for the LSN-peptide), Pep2 (for the LKSpeptide), and Pep3 (for the VIP-peptide) for the remainder of this study. Pep1 is located in the PolyS region near the N-terminus, and Pep3 and Pep2 are within the PolyS/T region downstream of the DELLA domain. All three phosphorylated sequences in RGA are not conserved among DELLAs (Supplementary Fig. 3). Interestingly, in the sly1 background with elevated GAs, phosphorylation in Pep1 was dramatically reduced (5.2% in sly1 vs. 30.5% in ga1), while phosphorylation in Pep2 was similar to that in ga1 (23.4% in sly1 vs. 28.6% in ga1, Table 1). MS analysis identified four mapped phosphosites in RGA and at least three additional sites that were located in specific peptides although the precise amino acid could not be mapped (Fig. 2a, b and Supplementary Table 1). As shown in Supplementary Table 1, Pep1 contains three mapped sites, Pep3 contains two unmapped sites, and Pep2 contains two sites (only one was mapped). None of these RGA phosphosites have been identified or analyzed by previous RGA functional studies⁴².





rga^{m2D}: LKSCDDPDDMVEDEDEGTQIG

rga^{m2A}: LKSCAAPDAMVAAAAAGTOIG

rga^{m1A}: LSNHGAAAAAAIAK

rga^{m1D}: LSNHGEDDDDDDDIDK

LKS-peptide (Pep 2) mutations

VIP-peptide (Pep 3) mutations rga^{m3A}: VIPGNAIYQFPAIDAAAAANNQNKR

Fig. 2 | **Identification of phosphorylation sites in RGA by LC-ESI-MS/MS. a** RGA phosphorylation sites identified by MS/MS. The schematic shows the RGA protein structure; two structurally disordered regions are indicated as solid black lines. The DELLA domain is shaded in pink. The LSN-peptide (Pep1) and LKS-peptide (Pep2) containing abundant phosphorylation are in bold (black letters). The S/T residues in green letters are confirmed phosphorylation sites. The underlined residues are amino acid stretches, in which one or more residues are modified (in addition to the identified sites), but the specific residues could not be mapped. The underlined K in parenthesis indicates the extra Lys residue in RGA GKG for creating an additional trypsin cleavage site. **b** Summary of PTM sites in RGA. Phosphorylated residues are in green as described in (**a**). *O*-fucosylated residues are in red, *O*-GlcNAcylated

residues in blue. Same color scheme was applied to the underlined regions, which are amino acid stretches, in which one or more residues are modified (in addition to the identified sites), but the specific residues could not be mapped. The underlined K in parenthesis indicates the extra Lys residue in RGA^{GKG}. **c** Mutated residues in rga^{mlA}, rga^{mlD}, rga^{m2A}, rga^{m2D} and rga^{m3A} are highlighted in orange. **d** Expression and phosphorylation pattern of P_{RGA} :His-FLAG-RGA/-rga ga1 dP transgenic lines using standard SDS-PAGE and Phos-tag (25 μ M) gels. Protein blots were probed with anti-FLAG antibody or anti-tubulin (TUB, as a loading control). Representative images of 3 biological repeats are shown. The mean ratios of phosphorylated RGA/unphosphorylated RGA/rga from 3 biological repeats are shown below the Phos-tag gel blot. –, not detectable. Source data are provided in the Source Data file.

RGA phosphorylation was not significantly altered by *spy* or *sec* mutation

The phosphorylation sites in RGA are located in the two disordered Sand S/T-rich sequences (flanking the DELLA domain, Fig. 2a), which were also shown previously to contain O-GlcNAc and O-Fuc sites, although most of the MS analyses were done using transiently expressed RGA in N. benthamiana^{31,32}. To investigate the interplay among these three PTMs in Arabidopsis, we identified RGA glycosylation sites and compared the relative abundances of each PTM in RGA^{GKG} purified from ga1-3, sly1-10, sly1-10 spy (two spy alleles, spy-12 and spy-19, were included), and sly1-10 sec-3 mutants. Each spy allele contains a point mutation that results in an amino acid substitution in its catalytic domain³², and sec-3 is a null allele due to transposon Ds insertion³¹. A summary of all PTM sites and their relative abundances is shown in Fig. 2b, Table 1 and Supplementary Table 1. All three PTMs were detected in Pep1, although O-GlcNAcylation and O-fucosylation were present at lower levels than phosphorylation. O-GlcNAcylation, but not O-fucosylation, was also identified in 4.2% of Pep2. Additionally, we found GVI-peptide (GVIGTTVTTTTTTTAAGESTR) that contains the poly-T track was highly O-GlcNAcylated (69.7% in ga1 and 58.4% in sly1), indicating that the levels of GlcNAcylation were not significantly altered by GA status. This is consistent with previous studies showing that transcript and protein levels of SPY and

SEC are not regulated by GA^{31,32}. We detected only very low levels of *O*-fucosylation in Pep1 and GVI-peptide due to technical limitations. Loss of *O*-Fuc moiety during purification is likely because no effective fucosidase inhibitors are available in contrast to well characterized inhibitors for phosphatases and *O*-GlcNAcase. In summary, phosphorylation is located mainly in Pep1 and Pep2, but also at low levels in Pep3. *O*-GlcNAcylation is highest in GVI-peptide (poly-T track), but is also present at low levels in Pep1 and Pep2. *O*-Fuc was only detected at very low levels in Pep1 and GVI-peptide (Fig. 2b, Table 1 and Supplementary Table 1).

In Pep1 that contains all three PTMs, phosphorylation was not affected by *spy*, although it was increased about 2-fold by *sec* (5.2% in *sly1* vs. 12.2% in *sly1 sec*) (Table 1). In contrast, phosphorylation levels in Pep2 remained similar in the presence or absence of *spy* or *sec* mutation (Table 1), suggesting that phosphorylation of Pep2 is not significantly affected by *O*-fucosylation or *O*-GlcNAcylation. *O*-GlcNAcylation in Pep1 was elevated -5-fold by *spy* (2.1% in *sly1* vs 9.5% in *sly1 spy*), whereas *O*-fucosylation was increased -3-fold by *sec*, indicating antagonistic interaction between *O*-GlcNAc and *O*-Fuc modifications.

Phosphorylation of Pep1 and Pep2 enhanced RGA activity

Our MS analysis identified two highly phosphorylated RGA peptides, Pep1 and Pep2. To investigate the role of phosphorylation on RGA

Table 1 | Relative abundances of posttranslational modifications in FLAG-RGA $^{\text{GKG}}$

Dontido/	Relative abundance ^a			
Peptide/ Modification	Relative apulicance			
	ga1-3 (%)	sly1-10 (%)	sly1 spy (%)	sly1 sec (%)
LSNHGTSSSSSSI	SK(DK) (Pep1)			
PO ₄	30.5	5.2	3.0	12.2
O-GlcNAc	1.9	2.1	9.5	0.0
O-Fuc	0.3	0.7	0.0	2.0
O-Hex ^b	0.0	0.1	0.1	0.0
VIPGNAIYQFPAID	SSSSSNNQNKR (I	Pep3)		
PO ₄	2.5	0.0	0.8	0.3
(LK)SCSSPDSMV1	STSTGTQIG <u>K</u> (Pe	p2)		
PO ₄	28.6	23.4	18.7	24.0
O-GlcNAc	3.7	4.2	4.7	0.0
O-Hex ^b	0.1	0.7	0.1	0.0
GVIGTTVTTTTTT	TAAGESTR			
O-GlcNAc	69.7	58.4	64.6	0.1
O-Fuc	0.4	0.4	0.0	0.3
O-Hex ^b	14.6	12.6	13.4	0.0

Peptide abundances were determined from ion currents taken from the MS1 survey scan. PTM levels are reported as the % of the total peptide abundance detected. Total abundances were calculated from ion currents observed in the MS1 mass spectra [(modified peptide ion current) / (sum of all modified peptides + unmodified peptide ion current)] × 100. The table shows average percentage values of peptides with PTMs as specified. The percentage values are average of three biological repeats for ga1-3 and sly1-10 or two biological repeats for sly1-10 sec-3. Percentage values for sly1 spy are the average of sly1-10 sly-12 and sly1-10 sly-19 samples.

The identity of this hexose has not been established, nor its biological function.

function, we generated transgenic Arabidopsis expressing four mutated rga proteins with the following mutations: rga^{m1A} (8 S/T-to-A in Pep1), rga^{m1D} (8 S/T-to-D/E in Pep1), rga^{m2A} (8 S/T-to-A in Pep2), or rga^{m2D} (8 S/T-to-D/E in Pep2) in the gal dP background (Fig. 2c), m1A and m2A should abolish phosphorylation of RGA Pep1 or Pep2, respectively, whereas m1D and m2D are phosphomimetic substitutions. Three independent homozygous transgenic lines for each construct $(P_{RGA}:His\text{-}FLAG\text{-}rga^{m1A}, P_{RGA}:His\text{-}FLAG\text{-}rga^{m1D}, P_{RGA}:His\text{-}FLAG\text{-}rga^{m2A},$ P_{RGA} :His-FLAG-rga^{m2D}) with similar expression levels as the P_{RGA} :His-FLAG-RGA lines were used for phenotype analysis (Supplementary Fig. 4a, b). As expected, His-FLAG-RGA restored the dwarf phenotype in ga1 dP. m1A only slightly decreased RGA's growth repression activity (Fig. 3a, b, Supplementary Fig. 4c, d), and did not reduce its overall phosphorylation levels (Fig. 2d). The phosphomimetic m1D also slightly reduced RGA's growth repression activity. In contrast, m2A completely abolished phosphorylation of RGA (Fig. 2d), and markedly reduced its growth repression (Fig. 3a, b, Supplementary Fig. 4c, d). The rga^{m2D} ga1 dP displayed similar dwarf phenotype as that of His-FLAG-RGA ga1 dP. These results indicate that Pep2 phosphorylation appears to play a more major role in promoting RGA activity than Pep1. To examine the role of Pep3 phosphorylation, we also generated rga^{m3A} (5 S-to-A in Pep3) in the gal dP background. Consistent with the low levels of phosphorylation in Pep3, rga^{m3A} did not impair RGA activity (Supplementary Fig. 5). The m1D and m2D did not confer opposite effects compared to m1A and m2A, respectively. These results are not surprising because Asp/Glu substitutions do not always capture the phosphorylation function due to size and charge differences⁴⁸.

Hypocotyl elongation assays using representative *His-FLAG-RGA/rga* lines in the *ga1 dP* background further showed that only *His-FLAG-rga*^{m24} conferred much elevated GA responses comparing to *His-FLAG-RGA* (Fig. 3c, d). We also compared activities of rga^{m2A}, rga^{m2D} and RGA in regulating transcript levels of ten selected RGA target genes^{21,49,50}, including five RGA-activated genes (*SCL3, GID1B, Exp-PT1, IQD22* and *GA2OOX2*) and five RGA-repressed genes (*IAA16, EXP8, GH3.3, SAUR16*

and PMEI13) by RT-qPCR analysis. Consistent with the whole plant phenotype results, His-FLAG-rga^{m2A} showed reduced activity while His-FLAG-rga^{m2D} displayed similar activity as His-FLAG-RGA in upregulating or downregulating these target genes, respectively (Fig. 3e. f). These results indicate that Pep2 phosphorylation promotes RGA activity more strongly. To examine the combined effect of abolishing phosphorylation of both Pep1 and Pep2, we generated transgenic lines expressing His-FLAG-rga^{m12A} with both *m1A* and *m2A* mutations in the gal dP background. In the T1 generation, m12A resulted in further lowering growth suppression activity of RGA in comparison to m2A (Supplementary Fig. 6a-c), supporting that combined mutations abolishing phosphorylation in both Pep1 and Pep2 additively reduced RGA activity. We further compared the activities of RGA and rga mutant proteins on inducing target gene SCL3 expression by a dual luciferase (LUC) assay using the transient expression system in Nicotiana benthamiana^{51,52}. The P_{SCI,3}:firefly LUC (fLUC) was used as the reporter for this assay, and 35S:Renilla LUC (rLUC) was the internal control to normalize variations in transformation efficiency. The effectors included 35S:FLAG-RGA and 35S:FLAG-rga constructs. As expected, when co-expressed with FLAG-RGA, PSCI3:fLUC expression was induced about 13-fold compared to the negative control (Supplementary Fig. 6d, e). The m1A and m2A mutations exhibited additive effects in reducing RGA transactivation activity (Supplementary Fig. 6d, e), consistent with the phenotypes of the corresponding mutant plants (Supplementary Fig. 6b, c).

Pep2 phosphorylation did not affect RGA protein stability or interaction with PIFs or BZR1

To investigate how Pep2 phosphorylation enhances RGA function, we first examined the effects of rga^{m2A} and rga^{m2D} mutations on its subcellular localization and stability. Protein fractionation and immunoblot analysis showed that rga^{m2A} or rga^{m2D} did not alter nuclear localization or GA-induced degradation of RGA in Arabidopsis (Supplementary Fig. 7). Similarly, rga^{miA} or rga^{miD} did not affect RGA stability (Supplementary Fig. 7b. c). Considering that O-Fuc and O-GlcNAc modifications oppositely alter RGA interactions with transcription factors PIFs and BZR131,32, we tested whether rgam2A reduced binding to PIF3 or BZR1. In vitro pulldown assays were performed using recombinant GST-tagged PIF3 and BZR1, and protein extracts from transgenic Arabidopsis expressing His-FLAG-RGA, His-FLAG-rgam2A or His-FLAG-rga^{m2D} (Fig. 4a, Supplementary Fig. 8). However, GST-PIF3 and GST-BZR1 pulled down His-FLAG-RGA, -rga^{m2A} and -rga^{m2D} similarly (Fig. 4a), suggesting that phosphorylation of Pep2 regulates DELLA function differently from O-glycosylation.

Pep2 phosphorylation increased H2A binding at target chromatin

We recently found that interaction with histone H2A is essential for RGA activity by promoting the formation of the TF-RGA-H2A complex at the target chromatin²¹. Importantly, rga^{m2A} showed reduced affinity to H2A by co-IP assays (Fig. 4b), supporting that phosphorylation of Pep2 enhances RGA-H2A interaction in planta. In addition, histones H3 and H4 also co-immunoprecipitated with FLAG-RGA, along with H2A (Fig. 4b), indicating that RGA mainly interacted with H2A in the nucleosomes instead of the "free" H2A. The co-IP assay using rga^{m2A} showed very weak H3 and H4 signals by immunoblot analysis, consistent with its weak interaction with H2A (Fig. 4b). On the other hand, rgamlA did not show detectable reduction in H2A binding (Fig. 4c). ChIP-qPCR analysis was also performed using transgenic lines containing P_{RGA}:His-FLAG-RGA or -rga in the ga1 dP background, and showed that FLAG-rga^{m2A} significantly reduced association with four selected target promoters, including two RGA-activated genes (SCL3 and GID1B) and two RGA-repressed genes (IAA16 and EXP8) (Fig. 4d). In contrast, His-FLAG-rga^{m2D} displayed similar association with target promoters as His-FLAG-RGA. These results provide strong evidence for

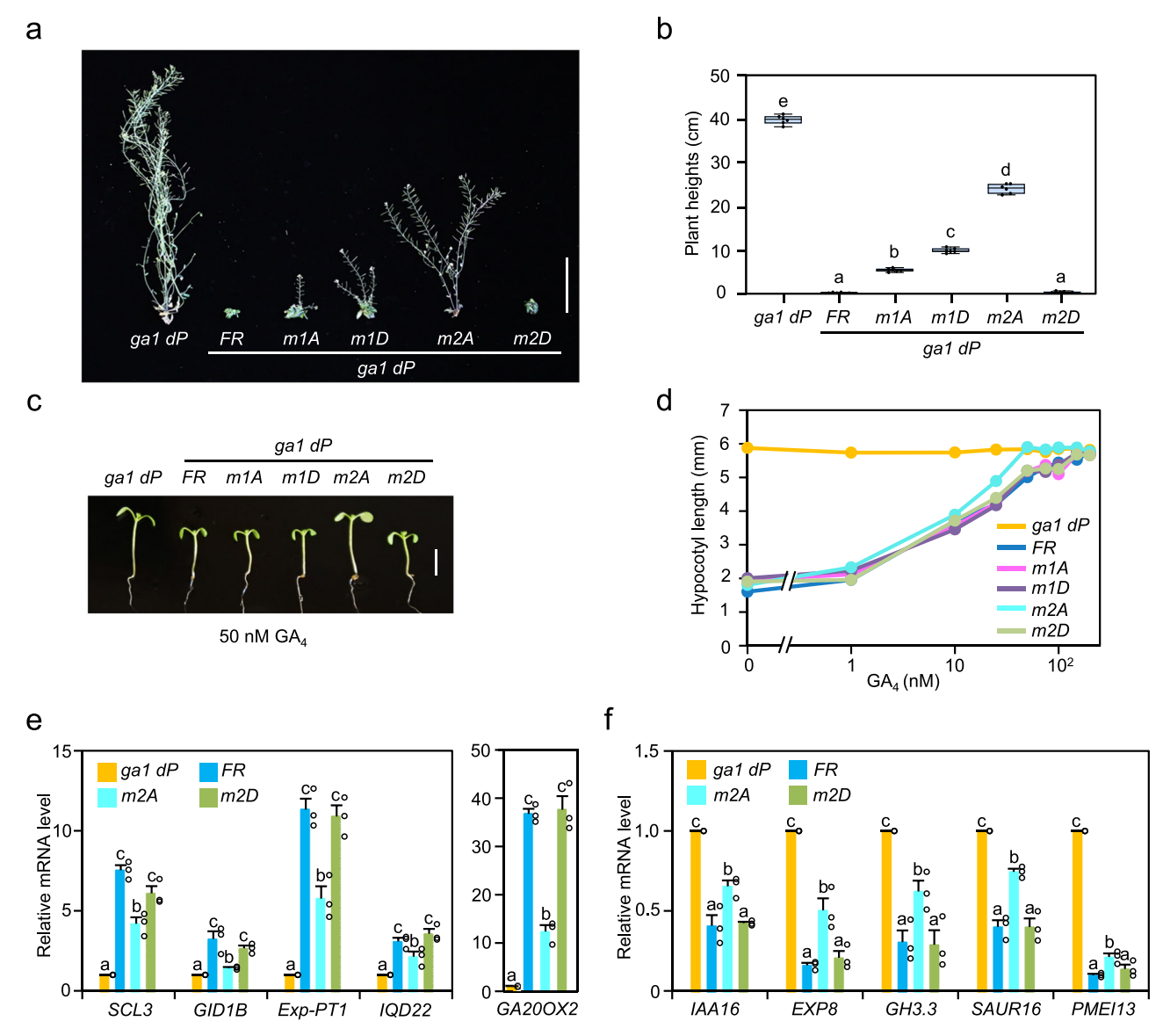


Fig. 3 | **Phosphorylation of RGA in Pep 2 enhances RGA function. a**, **b** Phenotypes of His-FLAG-RGA/rga transgenic lines. In (**a**), Representative 55-d-old plants under LD conditions. FR (#5), m1A (#3), m1D (#3), m2A (#4) and m2D (#7). Bar = 10 cm. In (**b**), Boxplot showing final heights of different lines as labeled. n = 6. Center lines and box edges are medians and the lower/upper quartiles, respectively. Whiskers extend to the lowest and highest data points within 1.5× interquartile range (IQR) below and above the lower and upper quartiles, respectively. Different letters above the bars represent significant differences (p < 0.01) as determined by two-tailed Student's t tests. The phenotypic analysis was repeated three times with similar results. **c**, **d** *His-FLAG-rga*^{m2A} ga1 dP displayed an enhanced

GA response in hypocotyl growth. Seedlings were grown in medium containing varying concentrations of GA₄. Hypocotyl lengths were measured at day 9. Bar = 3 mm. In (**d**), Average hypocotyl lengths. Means \pm SE are listed in the Source Data file. n = 11-12. Exact n and p values for (**b**) and (**d**) are listed in the Source Data file. The assay was repeated three times with similar results. **e**, **f** RT-qPCR showing rga^{m2A} caused reduced expression of RGA-induced genes (**e**) and increased expression of RGA-repressed genes (**f**). *PP2A* was used to normalize different samples. Means \pm SE of three biological replicates are shown. Different letters above the bars represent significant differences (p < 0.05) by two-tailed Student's t-test. Source data are provided in the Source Data file.

the promoting role of RGA Pep2 phosphorylation in binding H2A at target chromatin.

The PFYRE subdomain within the RGA GRAS domain is essential for H2A interaction because single amino acid substitutions in this region result in markedly reduced H2A binding affinity in planta²¹. Considering that Pep2 is in the PolyS/T region linking the DELLA domain and the GRAS domain of RGA, it is possible that phosphorylation of Pep2 may induce a conformational change to make the PFYRE subdomain more accessible for H2A binding. Alternatively, the PolyS/T region may also directly involve in H2A binding. Co-IP assays were performed using *N. benthamiana* that transiently expressed full-length (FL) or truncated FLAG-RGA proteins together with Myc-H2A or Myc-GFP as a negative control. As expected, both the FL-RGA and

C-terminal RGA fragment (CT3) that includes the PFYRE subdomain were co-immunoprecipitated with Myc-H2A (Fig. 5). Notably, the N-terminal RGA fragments (NT2 and NT3) that include the PolyS/T region were also co-immunoprecipitated with Myc-H2A, whereas RGA-NT1 lacking the PolyS/T region was not (Fig. 5). These results indicate that both PolyS/T and PFYRE regions play important roles for H2A binding.

Discussion

In this study, we showed that phosphorylation of the RGA Pep2 in the PolyS/T region enhanced RGA-H2A interaction and RGA association with target promoters, while it did not affect RGA interaction with transcription factors PIF3 and BZR1. This conclusion is based on (1)

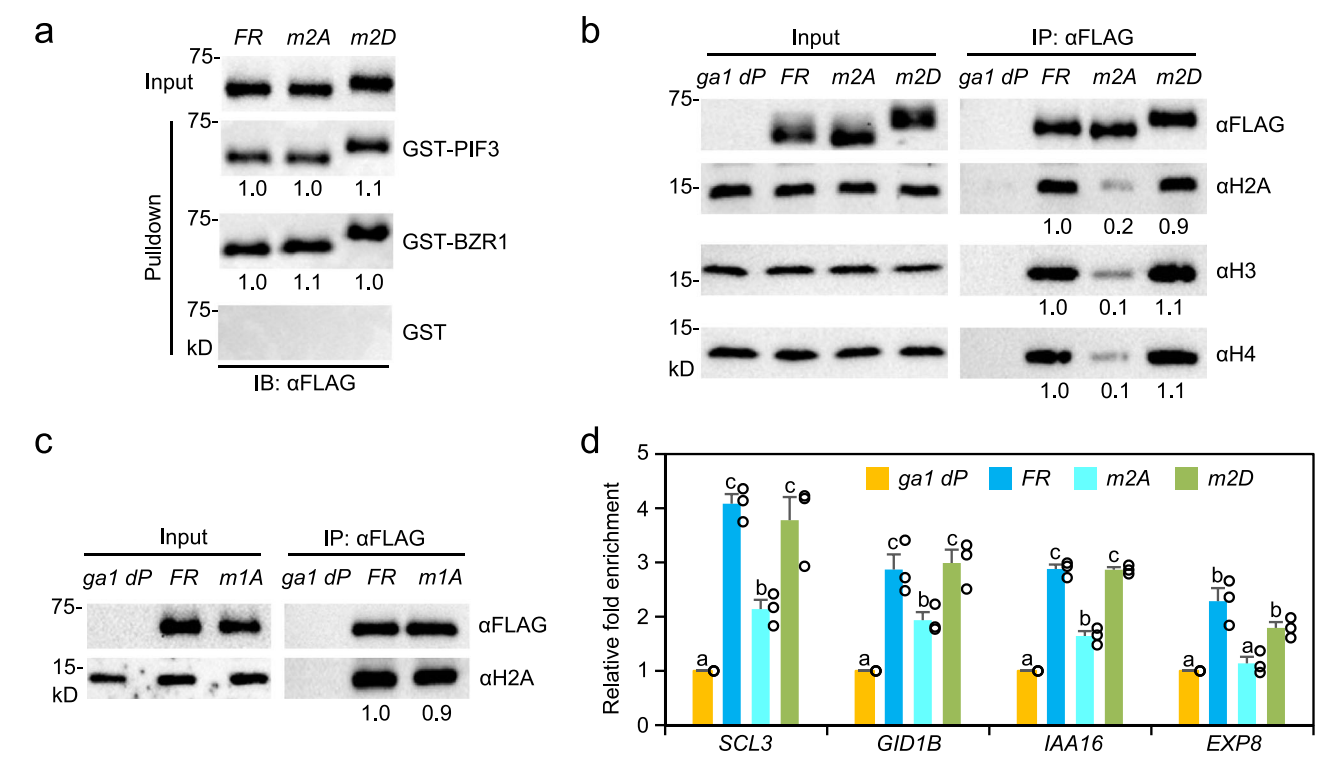


Fig. 4 | **Phosphorylation promoted RGA interaction with H2A, but did not affect TF binding. a** In vitro pulldown assay showing rga^{m2A} and rga^{m2D} did not affect binding to PIF3 or BZRI. Recombinant GST, GST-PIF3 and GST-BZRI bound to glutathione–Sepharose beads were used separately to pull down His-FLAG-RGA/rga from protein extracts from transgenic *Arabidopsis* in the *ga1 dP* background. Immunoblots containing input *Arabidopsis* extracts and pulldown samples were detected with an anti-FLAG antibody. PS-stained blots indicated that similar amounts of the GST/GST-fusion proteins were used in each set of the pulldown assays (Supplementary Fig. 8). Representative images of two biological repeats are shown. Relative amounts of His-FLAG-RGA/rga pulled down by GST fusion proteins are shown. The levels of His-FLAG-RGA were set as 1.0. **b, c** Co-IP assays showing that rga^{m2A} reduced binding to H2A, H3 and H4, whereas rga^{m1A} did not affect H2A interaction. His-FLAG-RGA/rga from protein extracts of transgenic *Arabidopsis* (in *ga1 dP* background) carrying P_{RGA} -His-FLAG-RGA/rga were immunoprecipitated

using an anti-FLAG antibody. Immunoblots containing input *Arabidopsis* extracts and IP eluate samples were detected with anti-FLAG, H2A, H3 and H4 antibodies, separately. Representative images of two or three biological repeats are shown. In **b**, **c**, relative amounts of H2A/H3/H4 co-immunoprecipitated with FLAG-RGA/rga are shown. **d** ChIP-qPCR analysis showing rga^{m2A} reduced association with target chromatin. ChIP was performed using transgenic lines containing P_{RGA} :*FLAG-RGA/rga* in the *ga1 dP* background as labeled. The parental line *ga1 dP* was included as a control. Two RGA-activated genes (*SCL3* and *GID1B*) and two RGA-repressed genes (*IAA16* and *EXP8*) were tested by qPCR using primers near the RGA binding peaks. The relative enrichment fold was calculated by normalizing against ChIP-qPCR of non-transgenic *ga1 dP* control using *PP2A*. Means \pm SE of three biological replicates are shown. Different letters above the bars represent significant differences (p < 0.05) by two-tailed Student's t-test. Source data are provided in the Source Data file.

direct detection of RGA phosphorylation sites in planta by MS/MS analysis; (2) in vivo functional analysis of FLAG-RGA vs FLAG-rga mutant proteins; and (3) in vivo co-IP and ChIP-qPCR assays. We recently showed that the PFYRE subdomain within the RGA GRAS domain is essential for H2A binding, while the LHR1 subdomain is required for interaction with TFs²¹. Here we demonstrated that both PolyS/T and PFYRE regions play important roles for H2A binding. We further showed that RGA interacts with H2A in the nucleosomes, and that phosphorylation of Pep2 enhances RGA-H2A binding. The rga^{m2A} mutant protein abolishes RGA phosphorylation, and may adopt a different protein conformation that interferes with H2A binding (Fig. 6).

Our MS analysis showed that both Pep1 and Pep2 in RGA contained high levels of phosphorylation in the GA-deficient *ga1* background. In addition to this study, phospho-proteomics studies also identified phosphorylation within RGA Pep1, although its role had not been investigated^{53–55}. Conversely, phosphorylation of Pep2 has not been reported previously because this peptide could only be detected using the *RGA*^{CKG} transgene. Although *m1A* mutation that abolished phosphorylation of Pep1 only slightly reduced RGA activity in planta, it had an additive effect when combined with *m2A* to downregulate RGA activity (Supplementary Fig. 6). Importantly, phosphorylation in Pep1 was much reduced in the *sly1* mutant containing elevated GAs compared to *ga1*, suggesting that GA promotes dephosphorylation of RGA to reduce its activity. The mechanism how GA downregulates RGA

phosphorylation requires further studies. One possibility would be through regulation of the unidentified protein kinase(s). Although expression of the CK1 protein kinase, EL1, was shown to be downregulated by GA in rice⁴¹, our results indicate that higher order mutations in the Arabidopsis EL1 homologs (AEL1-4) did not reduce RGA phosphorylation. Consistent with our results, a recent phosphoproteomics study using Arabidopsis AEL overexpression lines and triple ael mutants did not identify any DELLA proteins as the substrates of these kinases⁵⁶. While preparing our manuscript, a GSK3/SHAGGY-like kinase-encoding gene GSK3 in Triticum aestivum (wheat) was reported to phosphorylate DELLA (Rht-B1b)⁵⁷, although Rht-B1b phosphorylation by GSK3 has not been demonstrated in planta. Three phosphorylation sites in Rht-B1b located between the DELLA and GRAS domains (Supplementary Fig. 3) were identified by in vitro enzyme reactions in the presence of GSK3, followed by MS analysis. Ser-to-Ala substitutions at all three phosphorylation sites led to reduced Rht-B1b activity in transgenic wheat, which is consistent with our finding that Ala substitutions in RGA Pep2 reduced RGA activity. However, their in vitro protein degradation assay further suggested that phosphorylation also stabilizes Rht-B1b⁵⁷. This contrasts with our results showing that Ala substitutions in RGA Pep2 did not alter its stability in planta. GSK3 in wheat is an ortholog of BRASSINOSTEROID INSENSITIVE 2 (BIN2) in Arabidopsis⁵⁷, which is a negative regulator of BR signaling, and BR activates its signaling pathway by inducing BIN2 degradation⁵⁸. We

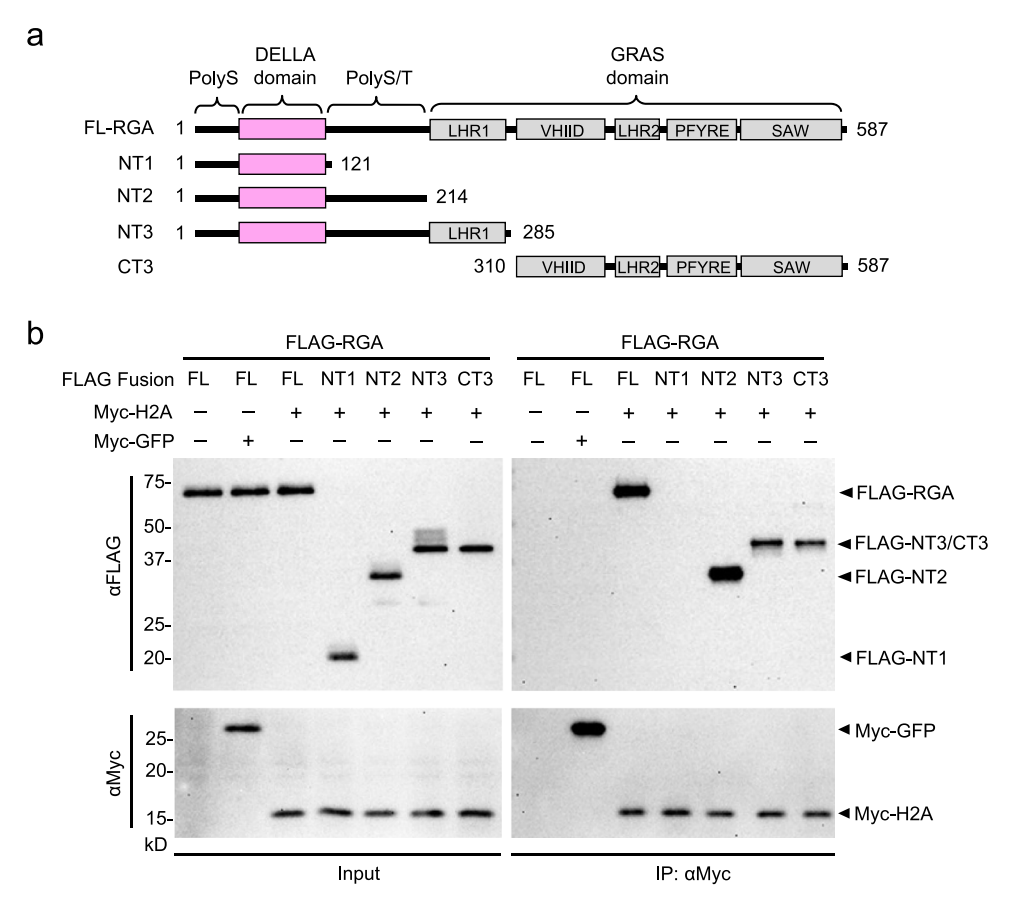


Fig. 5 | **H2A** binds to both the PolyS/T region and GRAS domain of RGA. a Schematics of full-length (FL) and a series of truncated RGA proteins. LHR, Leucin heptad repeat. **b** Co-IP assays showed that both PolyS/T and GRAS domain interacted with H2A. FLAG-RGA (FL or truncated) was expressed alone (–) or coexpressed with Myc-H2A in *N. benthamiana*. Myc-GFP was included as a negative control. Myc-H2A or -GFP were immunoprecipitated using anti-Myc agarose. Left

panel (Input): Immunoblots containing total protein extracts. Right panel (α Myc immunoprecipitated samples): Immunoblots containing IP eluates were probed with α FLAG or α Myc as labeled. Representative images of 2 biological repeats are shown. Predicted molecular masses for FLAG-NT3 and FLAG-CT3 are 37 kD and 35 kD, respectively. Source data are provided in the Source Data file.

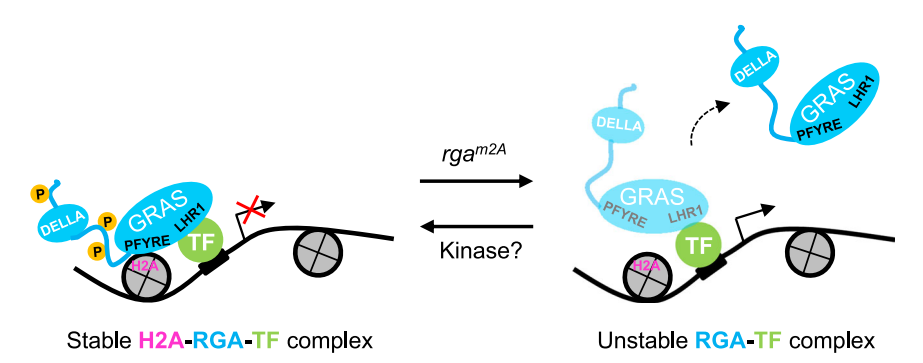


Fig. 6 | **Proposed model for the regulatory role of RGA phosphorylation.** RGA is recruited to target chromatin by interaction with TFs via the LHR1 subdomain, which is then stabilized by binding to H2A via its PolyS/T region and the PFYRE subdomain to form H2A-RGA-TF complexes. Phosphorylation of the Pep 2 within the PolyS/T region between the DELLA domain and the GRAS domain by unidentified kinase(s) enhances RGA-H2A binding. The rga^{m2A} mutant protein abolishes RGA phosphorylation, and adopts a different protein conformation that

interferes with H2A binding. This leads to unstable transient TF-rga^{m2A} interaction, and disassociation of rga^{m2A} from the target chromatin. The diagram only depicts RGA-mediated transcription repression. A similar diagram can depict RGA-mediated transcription activation, except that the H2A-RGA-TF complex will promote transcription of target genes and that dephosphorylation by rga^{m2A} will reduce transcription. Figure modified from Huang et al.²¹.

showed that BR treatment does not reduce RGA stability⁵⁹ or phosphorylation levels in *Arabidopsis* (Supplementary Fig. 2), suggesting that RGA is unlikely to be phosphorylated by BIN2.

The phosphorylation sites identified in RGA are located within the disordered PolyS and PolyS/T regions that flank the DELLA domain.

Although these phosphorylation sites in RGA are not conserved among DELLAs, all DELLAs contain at least the PolyS/T region (Supplementary Fig. 3). These results suggest that phosphorylation of the disordered PolyS and/or PolyS/T regions alters the conformation of DELLAs to promote H2A binding.

In summary, our study has uncovered a key role of phosphorylation in enhancing DELLA activity by promoting DELLA-H2A interaction at target chromatin. This adds a third posttranslational regulatory mechanism to modulate DELLA activity, in addition to protein stability (by ubiquitination and SUMOylation) and binding affinity to TFs (by *O*-GlcNAc and *O*-Fuc modifications). Identification of protein kinase(s) for RGA phosphorylation in *Arabidopsis* will help reveal the internal and/or external cues that trigger DELLA phosphorylation. Furthermore, structural analysis of phosphorylated vs. unphosphorylated RGA will help to further elucidate the molecular mechanism of DELLA-mediated transcription reprogramming.

Methods

Plant materials, growth conditions, and generation of transgenic lines

In most experiments, Arabidopsis plants were grown in the growth room under long-day (LD) conditions (16 h light, 22 °C; 8 h dark, 20 °C). The ga1-13, sly1-10 (bc 6x Col-0), and ga1-13 della pentuple (ga1 dP) are in the Col-0 background^{21,50}. The ga1-3 rga-24 and sly1-10 rga-24 double mutants are in the Ler background³¹. The mlk1 (SALK 026482), mlk2 (SALK 035080), mlk3 (SALK 017102) and mlk4 (SALK 1615), all in the Col-O background, were obtained from the Arabidopsis Biological Resource Center (https://abrc.osu.edu/). The double and triple homozygous mlk mutants were generated by crosses. Transgenic Arabidopsis lines, P_{RGA}:His-FLAG-RGA ga1-13 della pentuple (ga1 dP), P_{RGA}:His-FLAG-RGA^{GKG} in ga1-3 rga-24, sly1-10 rga-24 or sly1-10 sec-3 rga-24, and the P_{BZRI} :BZR1-CFP line were reported previously^{21,31,32,59}. P_{RGA}:His-FLAG-RGA^{GKG} in sly1-10 spy-12 rga-24 or sly1-10 spy-19 rga-24 were generated by crosses between P_{RGA} :His-FLAG-RGA^{GKG} in sly1-10 rga-24 and different spy alleles. pRGA-His-3xFLAG-RGA, pRGA-His-3xFLAG-m1A, pRGA-His-3xFLAG-m1D, pRGA-His-3xFLAG-m2A, pRGA-His-3xFLAG-m2D, pRGA-His-3xFLAG-m12A, pRGA-His-3xFLAG-m3A constructs were introduced into ga1-13 dP by agrobacteriummediated transformation. Independent transgenic lines with single insertion were selected by Basta resistance. Multiple independent transgenic lines (6 to 9) for each construct were screened by standard SDS-PAGE gel blot analysis to select for lines that expressed His-FLAG-RGA or -rga protein at similar levels. The *P_{RGA}:His-FLAG-RGA* transgenic lines in the WT, mlk double and triple mutant backgrounds were generated by transformation. Transgenic lines for each genetic background that expressed similar levels of His-FLAG-RGA were used for further analysis.

Plasmid construction

The following plasmids were described previously: P_{SCL3} fLUC, and $35S:rLUC^{52}$ for dual LUC assays, pEG3F-RGA (35S:FLAG-RGA) and pEG2O3-H2A (35S:MYC-H2A)²¹ for transient expression in *N. benthamiana*, pBm43GW⁶⁰ for cloning, GST-PIF3, GST-BZRI³¹, and GST-H2A²¹ for expression in *E. coli*. Primers and plasmid constructs are listed in Supplementary Tables 2 and 3, respectively. All DNA constructs generated from PCR amplification were sequenced to ensure that no mutations were introduced. Construction of pRGA-His-3xFLAG-RGA/m1A/m1D/m2A/m2D/m12A/m3A were generated using four constructs: J035 (RGA promoter, 8.1 kb), pBm43GW⁶⁰, J015(RGA 3'UTR) and pDONR2O7-His-3XFLAG-RGA/m1A/m1D/m2A/m2D/m12A/m3A by Gateway LR reaction.

Phenotype analyses

For final height measurement, the seeds of parental line $ga1\ dP$, and transgenic lines carrying P_{RGA} :His-FLAG-RGA/rga (all in the $ga1\ dP$ background) were treated with $10\ \mu M\ GA_4$ for 3 days at $4\ ^{\circ}C$, washed 6 times with water, and then were sown in soil under LD. The experiment was repeated 3 times for all, except rga^{m3A} was repeated 2 times, with similar results. For hypocotyl elongation analysis, surface-sterilized seeds were treated with $10\ \mu M\ GA_4$ for 3 days at $4\ ^{\circ}C$, washed 6 times

with water, and were plated on 0.5x Murashige and Skoog (MS) medium supplemented with different concentrations of GA₄ for 9 days under LD conditions (16 μ mol m-2 s-1 white light). Hypocotyl lengths were measured using ImageJ software (http://rsb.info.nih.gov/ij). Each experiment was performed at least three times with similar results and one set of representative results is shown.

Statistics and reproducibility

Statistical analyses were performed for all quantitative data using Excel, and significant differences determined by Student's *t*-tests. No statistical method was used to predetermine sample size. No data were excluded from the analyses; The experiments were not randomized; Investigators were not blinded to allocation during experiments and outcome assessment. Sample sizes were specified in the figure legends and Source Data file.

Reverse transcription (RT)-quantitative PCR (qPCR) and immunoblot analyses

Total RNA was extracted using the Quick-RNA MiniPrep kit (Zymo Research), and Reverse transcription was performed using Transcriptor First Strand cDNA Synthesis Kit (Roche) with anchored oligo dT₁₈. RT-PCR analysis was performed using the FastStart Essential DNA Green Master mix and LightCycler 96 (Roche Applied Science). Relative transcript levels were determined by normalizing with *PP2A* (Atlg13320)⁶¹. Primers for the qPCR are listed in Supplementary Table 2. Primers for *SCL3*, *GID1B*, *EXP8*, *SAUR16*, and *GH3.3* were reported previously⁵⁰.

For immunoblot assays, total proteins were extracted from 10 days-old seedlings using the 2×SDS extraction buffer (125 mM Tris-HCl pH 8.8, 4% SDS, 20% glycerol, 5% 2-Mercaptoethanol). Immunoblot analyses were performed using rat anti-RGA antiserum (DUR18, 1:1,000)⁵, horseradish peroxidase (HRP)-conjugated anti-FLAG M2 mouse monoclonal (Sigma Aldrich A8592, 1:10,000 dilution), rabbit anti-H3 polyclonal antibody (Abcam ab1791, 1:5,000 for Supplementary Fig. 7 or 1:1000 dilution for Fig. 4b), mouse anti-tubulin antibody (Sigma T5168, 1:100.000), rabbit anti-H2A monoclonal antibody (Abcam ab177308, 1:1,000 dilution), rabbit anti-H4 monoclonal antibody (Abcam ab222763, 1:1,000 dilution), mouse anti-GFP antibody (Roche 11814460001, 1:1,000 dilution) and mouse HRP-anti-MYC monoclonal antibodies (BioLegend 626803, 1:2000 dilution). HRP-conjugated donkey anti-mouse IgG (Jackson ImmunoResearch #715-035-150, 1:10,000 dilution) was used for anti-tubulin and anti-GFP. HRP-conjugated goat anti-rabbit IgG (Thermo-Fisher #31462, 1:10,000 dilution) was used to detect anti-H2A, anti-H3, and anti-H4. HRP-conjugated goat anti-rat IgG (Pierce #31470, 1:6000) was used for anti-RGA (DUR18). Chemiluminescent signals were detected by iBright FL1500 (Invitrogen).

Phos-tag mobility shift assay

Total proteins of 10-days-old seedlings were extracted from ground samples using the extraction buffer (50 mM Tris-HCl, pH 7.5, 150 mM NaCl, 0.5% Triton X-100, 1x Complete –EDTA free protease inhibitors). The proteins were separated in a 6% SDS–PAGE gel containing 25 μ M Phos-tag Acrylamide reagent (FUJIFILM Wako Chemicals USA Corp. #AAL-107) and 50 mM MnCl $_2$ following the manufacturer's instructions. After electrophoresis at 4 °C, the gel was washed 3 times with transfer buffer without methanol plus 5 mM of EDTA, rinsed once with transfer buffer, and then transferred to nitrocellulose membranes for immunoblot analysis.

In vitro pulldown and co-IP assays

In vitro pulldown assay was performed following the procedures published previously^{21,31}. Recombinant proteins (GST, GST-BZR1, and GST-PIF3) expressed in BL21-CodonPlus (DE3)-RIL (Agilent Technologies) were purified using glutathione beads. GST and GST-fusion proteins bound to glutathione beads were then used separately to pull

down FLAG-RGA/rga from protein extracts of transgenic *Arabidopsis* (in ga1 dP background) carrying P_{RGA} :FLAG-RGA/rga.

For in vivo co-IP assays, total protein complexes were extracted from *Arabidopsis* and immunoprecipitated using anti-FLAG-M2-Agarose beads as described²¹. Samples were analyzed by SDS-PAGE and immunoblotting using anti-FLAG-HRP antibody (Sigma–Aldrich, 1:10,000), anti-H2A antibody (Abcam ab177308), anti-H3 antibody (Abcam ab1791) and anti-H4 antibody (Abcam ab222763). Quantitative analysis of the relative signal intensity was performed using Imagel software (http://rsb.info.nih.gov/ij) or iBright FL1500 Imaging System.

For mapping RGA interaction domains with H2A, FLAG-RGA, FLAG-RGA(NT1), FLAG-RGA(NT2), FLAG-RGA(NT3), FLAG-RGA(CT3) and MYC-H2A were transiently expressed in *N. benthamiana* leaves. Co-IP assays were performed using rabbit anti-Myc polyclonal antibody-conjugated agarose beads (A7470; Sigma-Aldrich), as described previously³¹.

Transient expression and dual luciferase assay in *N. benthamiana*

The dual luciferase assays in *N. benthamiana* were performed as described previously using dual-luciferase reporter assay system⁵² except that leaves were harvest after 48 h of Agro-infiltration. At least three biological repeats were conducted for each effector combination.

Protein purification for MS analysis

His-FLAG-RGA was purified from P_{RGA} :HisFLAG-RGA^{GKG} transgenic Arabidopsis rga-24 lines with ga1-3 (n = 3), sly1-10 (n = 3), sly1-10 sec-3 (n = 2), sly1-10 spy-12 (n = 1) or sly1-10 spy-19 (n = 1), following the tandem affinity purification procedures described previously³².

Identification of PTM sites by online liquid chromatography tandem MS (MS/MS) analyses

Affinity-purified His-FLAG-RGA^{GKG} proteins extracted from *Arabidopsis* were trypsin-digested, and peptides were analyzed by online LC-electrospray ionization (ESI) tandem MS [electron-transfer dissociation (ETD) and collisionally activated dissociation (CAD) MS/MS] using a Thermo™ Orbitrap Fusion™ Tribrid™ mass spectrometer equipped with ETD^{32,62}. MS1 spectra were acquired in the Orbitrap with a resolution of 120,000, followed by low resolution data dependent MS2 analysis. Precursors of charge 2–6 were fragmented by CAD (30% normalized collision energy), and precursors of charge state 3–6 were fragmented using ETD with calibrated charge-dependent reaction times. Dynamic exclusion was included (repeat count of 1, repeat duration of 30 s, exclusion duration of 10 s).

Protein Metrics Byonic[™] (v3.11.3)⁶³ was used to search data against a database containing the UniProt Reviewed⁶⁴ entries for Arabidopsis thaliana proteins with the addition of the sequence for 6His-3xFLAG-RGA^{GKG}. Search settings included fully specific tryptic digestion, 3 potential missed cleavages, 10 ppm precursor mass tolerance, and 0.35 Da fragment mass tolerance. Alkylation of Cys residues was a fixed modification. Variable modifications included phosphorylation of Ser, Thr, and Tyr, O-fucosylation of Ser and Thr, O-GlcNAcylation of Ser and Thr, O-hexosylation of Ser and Thr, oxidation of Met, and the absence of alkylation on Cys. No manual cutoff based on false discovery rate or peptide score was applied. Byonic peptide-MS2 spectra matches were manually validated using both MS1 and MS2 spectra, and the modification site localization was confirmed by manual inspection of the MS2 spectra. Each peptide was quantified by integrating peak areas for all detected charge states including 13 C isotopes for the two most abundant charge states.

Chromatin immunoprecipitation (ChIP)-qPCR

Transgenic *Arabidopsis* seedlings carrying pRGA-His-3xFLAG-RGA, pRGA-His-3xFLAG-m2A and pRGA-His-3xFLAG-m2D (in the *ga1 dP*

background) grown for 10 days were harvested and cross-linked in 1% formaldehyde solution for 20 min. ChIP-qPCR assay was performed using anti-FLAG-M2-Agarose beads (Sigma–Aldrich A2220) as described²¹. The relative enrichment was calculated by normalizing against *ga1 dP* control samples using *PP2A*⁶¹. Primers for the ChIP–qPCR are listed in Supplementary Table 2. Primers for *SCL3*, *GID1B*, *IAA16* and *EXP8* were reported previously²¹.

Multiple sequence alignment

Multiple sequence alignment of DELLA proteins from different species was performed using MultAlin⁶⁵.

Accession numbers

Sequence information for *Arabidopsis* genes included in this article can be found in the GenBank/EMBL data libraries under accession numbers *RGA* (AT2G01570), *SCL3* (AT1G50420), *GID1B* (AT3G63010), *IAA16* (AT3G04730), *EXP8* (AT2G40610), *IQD22* (AT4G23060), *GA20ox2* (*AT5G51810*), *Exp-PT1* (AT2G45900), *SAUR16* (AT4G38860), *GH3.3* (AT2G23170), *PMEI13* (AT5G62360), *PP2A* (AT1G13320), *MLK1* (AT5G18190), *MLK2* (AT3G03940), *MLK3* (AT2G25760), *MLK4* (AT3G13670), *SPY* (AT3G11540), *SEC* (AT3G04240), *H2A* (AT1G51060), *H3* (AT5G10400), *H4* (AT2G28740), *SLY1* (AT4G24210), *BZR1* (AT1G75080) and *PIF3* (AT1G09530).

Reporting summary

Further information on research design is available in the Nature Portfolio Reporting Summary linked to this article.

Data availability

The mass spectrometry proteomics data have been deposited to the ProteomeXchange Consortium via the PRIDE⁶⁶ partner repository with the dataset identifier PXD046004. All other data generated in this study are provided in the Supplementary Information, Supplementary Data files and Source Data file. Source data are provided with this paper.

References

- Sponsel, V. M. in Annual Plant Reviews Vol. 49 (eds P. Hedden & G. S. Thomas) 1–36 (Wiley, 2016).
- Ueguchi-Tanaka, M. et al. GIBBERELLIN INSENSITIVE DWARF1 encodes a soluble receptor for gibberellin. Nature 437, 693–698 (2005).
- 3. Shani, E., Hedden, P. & Sun, T. P. Highlights in gibberellin research: a tale of the dwarf and the slender. *Plant Physiol.* **195**, 111–134 (2024).
- Sasaki, A. et al. Accumulation of phosphorylated repressor for gibberellin signaling in an F-box mutant. Science 299, 1896–1898 (2003)
- McGinnis, K. M. et al. The Arabidopsis SLEEPY1 gene encodes a putative F-box subunit of an SCF E3 ubiquitin ligase. Plant Cell 15, 1120–1130 (2003).
- Hernández-García, J., Briones-Moreno, A., Dumas, R. & Blázquez, M.
 A. Origin of gibberellin-dependent transcriptional regulation by molecular exploitation of a transactivation domain in DELLA proteins. Mol. Biol. Evol. 36, 908–918 (2019).
- Sun, T. P. The molecular mechanism and evolution of the GA-GID1-DELLA signaling module in plants. *Curr. Biol.* 21, R338–R345 (2011).
- Daviere, J. M. & Achard, P. A pivotal role of DELLAs in regulating multiple hormone signals. *Mol. Plant* 9, 10–20 (2016).
- Van De Velde, K., Ruelens, P., Geuten, K., Rohde, A. & Van Der Straeten, D. Exploiting DELLA signaling in cereals. *Trends Plant Sci.* 22, 880–893 (2017).
- 10. Pysh, L. D., Wysocka-Diller, J. W., Camilleri, C., Bouchez, D. & Benfey, P. N. The GRAS gene family in Arabidopsis: sequence

- characterization and basic expression analysis of the SCARECROW-LIKE genes. Plant J. 18, 111–119 (1999).
- Tian, C., Wan, P., Sun, S., Li, J. & Chen, M. Genome-wide analysis of the GRAS gene family in rice and Arabidopsis. *Plant Mol. Biol.* 54, 519–532 (2004).
- Silverstone, A. L., Ciampaglio, C. N. & Sun, T.-p The Arabidopsis RGA gene encodes a transcriptional regulator repressing the gibberellin signal transduction pathway. Plant Cell 10, 155–169 (1998).
- Peng, J. et al. The Arabidopsis GAI gene defines a signalling pathway that negatively regulates gibberellin responses. Genes Dev. 11, 3194–3205 (1997).
- Griffiths, J. et al. Genetic characterization and functional analysis of the GID1 gibberellin receptors in Arabidopsis. *Plant Cell* 18, 3399–3414 (2006).
- Murase, K., Hirano, Y., Sun, T.-p & Hakoshima, T. Gibberellininduced DELLA recognition by the gibberellin receptor GID1. *Nature* 456, 459–463 (2008).
- Shimada, A. et al. Structural basis for gibberellin recognition by its receptor GID1. Nature 456, 520–523 (2008).
- Willige, B. C. et al. The DELLA domain of GA insensitive mediates the interaction with the GA INSENSITIVE DWARF1A gibberellin receptor of Arabidopsis. *Plant Cell* 19, 1209–1220 (2007).
- Nakajima, M. et al. Identification and characterization of Arabidopsis gibberellin receptors. *Plant J.* 46, 880–889 (2006).
- Lantzouni, O., Alkofer, A., Falter-Braun, P. & Schwechheimer, C. Growth-regulating factors interact with DELLAs and regulate growth in cold stress. *Plant Cell* 32, 1018–1034 (2020).
- 20. Thomas, S. G., Bláquez, M. A. & Alabadí, D. in *Annual Plant Reviews* Vol. 49 (eds P. Hedden & S. G. Thomas) 189–228 (Wiley, 2016).
- Huang, X. et al. The master growth regulator DELLA binding to histone H2A is essential for DELLA-mediated global transcription regulation. *Nat. Plants* 9, 1291–1305 (2023).
- Dill, A., Thomas, S. G., Hu, J., Steber, C. M. & Sun, T.-p The Arabidopsis F-box protein SLEEPY1 targets GA signaling repressors for GA-induced degradation. *Plant Cell* 16, 1392–1405 (2004).
- 23. Muangprom, A., Thomas, S. G., Sun, T. P. & Osborn, T. C. A novel dwarfing mutation in a green revolution gene from *Brassica rapa*. *Plant Physiol.* **137**, 931–938 (2005).
- Hirano, K. et al. Characterization of the molecular mechanism underlying gibberellin perception complex formation in rice. *Plant Cell* 22, 2680–2696 (2010).
- Blanco-Tourinan, N., Serrano-Mislata, A. & Alabadí, D. Regulation of DELLA proteins by post-translational modifications. *Plant Cell Physiol.* 61, 1891–1901 (2020).
- Sun, T. P. Novel nucleocytoplasmic protein O-fucosylation by SPINDLY regulates diverse developmental processes in plants. Curr. Opin. Struct. Biol. 68, 113–121 (2021).
- Mutanwad, K. V. & Lucyshyn, D. Balancing O-GlcNAc and O-fucose in plants. FEBS J. 289, 3086–3092 (2022).
- Olszewski, N. E., West, C. M., Sassi, S. O. & Hartweck, L. M. O-GlcNAc protein modification in plants: evolution and function. Biochim Biophys. Acta 1800, 49–56 (2010).
- Conti, L. et al. Small ubiquitin-like modifier protein SUMO enables plants to control growth independently of the phytohormone gibberellin. Dev. Cell 28, 102–110 (2014).
- Campanaro, A. et al. SUMO proteases OTS1 and 2 control filament elongation through a DELLA-dependent mechanism. *Plant Reprod.* 29, 287–290 (2016).
- 31. Zentella, R. et al. O-GlcNAcylation of master growth repressor DELLA by secret agent modulates multiple signaling pathways in Arabidopsis. *Genes Dev.* **30**, 164–176 (2016).
- Zentella, R. et al. The Arabidopsis O-fucosyltransferase SPINDLY activates nuclear growth repressor DELLA. Nat. Chem. Biol. 13, 479–485 (2017).

- 33. Hart, G. W. Nutrient regulation of signaling and transcription. *J. Biol. Chem.* **294**. 2211–2231 (2019).
- 34. Gomi, K. et al. GID2, an F-box subunit of the SCF E3 complex, specifically interacts with phosphorylated SLR1 protein and regulates the gibberellin-dependent degradation of SLR1 in rice. *Plant J.* **37**, 626–634 (2004).
- 35. Fu, X. et al. The Arabidopsis mutant sleepy1^{gar2-1} protein promotes plant growth by increasing the affinity of the SCF^{SLY1} E3 ubiquitin ligase for DELLA protein substrates. *Plant Cell* **16**, 1406–1418 (2004).
- 36. Itoh, H. et al. Dissection of the phosphorylation of rice DELLA protein, SLENDER RICE1. *Plant Cell Physiol.* **46**, 1392–1399 (2005).
- Fu, X. et al. Gibberellin-mediated proteasome-dependent degradation of the barley DELLA protein SLN1 repressor. *Plant Cell* 14, 3191–3200 (2002).
- Hussain, A., Cao, D., Cheng, H., Wen, Z. & Peng, J. Identification of the conserved serine/threonine residues important for gibberellinsensitivity of Arabidopsis RGL2 protein. *Plant J.* 44, 88–99 (2005).
- Wang, F. et al. Biochemical insights on degradation of Arabidopsis DELLA proteins gained from a cell-free assay system. *Plant Cell* 21, 2378–2390 (2009).
- 40. Qin, Q. et al. Arabidopsis DELLA protein degradation is controlled by a type-one protein phosphatase, TOPP4. *PLoS Genet.* **10**, e1004464 (2014).
- 41. Dai, C. & Xue, H. W. Rice early flowering1, a CKI, phosphorylates DELLA protein SLR1 to negatively regulate gibberellin signalling. *EMBO J.* **29**, 1916–1927 (2010).
- Wang, W. et al. The six conserved serine/threonine sites of REPRESSOR OF ga1-3 protein are important for its functionality and stability in gibberellin signaling in Arabidopsis. Planta 240, 763–779 (2014).
- Kinoshita, E., Kinoshita-Kikuta, E., Takiyama, K. & Koike, T. Phosphate-binding tag, a new tool to visualize phosphorylated proteins. *Mol. Cell Proteom.* 5, 749–757 (2006).
- Ariizumi, T., Murase, K., Sun, T.-p & Steber, C. M. Proteolysisindependent downregulation of DELLA repression in Arabidopsis by the gibberellin receptor GIBBERELLIN INSENSITIVE DWARF1. *Plant Cell* 20, 2447–2459 (2008).
- Chen, H. H., Qu, L., Xu, Z. H., Zhu, J. K. & Xue, H. W. EL1-like casein kinases suppress ABA signaling and responses by phosphorylating and destabilizing the ABA receptors PYR/PYLs in Arabidopsis. *Mol. Plant* 11, 706–719 (2018).
- 46. Wang, Z. et al. Osmotic stress induces phosphorylation of histone H3 at threonine 3 in pericentromeric regions of *Arabidopsis thaliana*. *Proc. Natl Acad. Sci. USA* **112**, 8487–8492 (2015).
- Ni, W. et al. PPKs mediate direct signal transfer from phytochrome photoreceptors to transcription factor PIF3. *Nat. Commun.* 8, 15236 (2017).
- 48. Chen, Z. & Cole, P. A. Synthetic approaches to protein phosphorylation. *Curr. Opin. Chem. Biol.* **28**, 115–122 (2015).
- Zentella, R. et al. Global analysis of DELLA direct targets in early gibberellin signaling in Arabidopsis. *Plant Cell* 19, 3037–3057 (2007).
- Park, J. et al. GA signaling requires chromatin remodeler PICKLE to promote vegetative growth and phase transitions. *Plant Physiol.* 173, 1463–1474 (2017).
- Zhang, Z. L. et al. SCARECROW-LIKE 3 promotes gibberellin signaling by antagonizing DELLA in Arabidopsis. *Proc. Natl Acad. Sci.* USA 108, 2160–2165 (2011).
- 52. Zhou, X. et al. The ERF11 transcription factor promotes internode elongation by activating gibberellin biosynthesis and signaling. *Plant Physiol.* **171**, 2760–2770 (2016).
- 53. Schonberg, A. et al. Identification of STN7/STN8 kinase targets reveals connections between electron transport, metabolism and gene expression. *Plant J.* **90**, 1176–1186 (2017).

- van Wijk, K. J., Friso, G., Walther, D. & Schulze, W. X. Meta-analysis of Arabidopsis thaliana phospho-proteomics data reveals compartmentalization of phosphorylation motifs. Plant Cell 26, 2367–2389 (2014).
- 55. Wang, X. et al. A large-scale protein phosphorylation analysis reveals novel phosphorylation motifs and phosphoregulatory networks in Arabidopsis. *J. Proteom.* **78**, 486–498 (2013).
- Qu, L., Liu, M., Zheng, L., Wang, X. & Xue, H. Data-independent acquisition-based global phosphoproteomics reveal the diverse roles of casein kinase 1 in plant development. Sci. Bull. 68, 2077–2093 (2023).
- 57. Dong, H. et al. GSK3 phosphorylates and regulates the green revolution protein Rht-B1b to reduce plant height in wheat. *Plant Cell* **35**, 1970–1983 (2023).
- Kim, T. W. & Wang, Z. Y. Brassinosteroid signal transduction from receptor kinases to transcription factors. *Annu Rev. Plant Biol.* 61, 681–704 (2010).
- Bai, M. Y. et al. Brassinosteroid, gibberellin, and phytochrome signalling pathways impinge on a common transcription module in Arabidopsis. Nat. Cell Biol. 14, 810–817 (2012).
- 60. Karimi, M., De Meyer, B. & Hilson, P. Modular cloning in plant cells. *Trends Plant Sci.* **10**, 103–105 (2005).
- Oh, E., Zhu, J. Y. & Wang, Z. Y. Interaction between BZR1 and PIF4 integrates brassinosteroid and environmental responses. *Nat. Cell Biol.* 14, 802–809 (2012).
- Udeshi, N. D., Compton, P. D., Shabanowitz, J., Hunt, D. F. & Rose, K. L. Methods for analyzing peptides and proteins on a chromatographic timescale by electron-transfer dissociation mass spectrometry. *Nat. Protoc.* 3, 1709–1717 (2008).
- Bern, M., Kil, Y. J. & Becker, C. Byonic: advanced peptide and protein identification software. *Curr. Protoc. Bioinforma.* 40, 13.20.11–13.20.14 (2012).
- 64. UniProt, C. UniProt: the universal protein knowledgebase in 2021. *Nucleic Acids Res.* **49**, D480–D489 (2021).
- 65. Corpet, F. Multiple sequence alignment with hierarchical clustering. *Nucleic Acids Res.* **16**, 10881–10890 (1988).
- 66. Perez-Riverol, Y. et al. The PRIDE database resources in 2022: a hub for mass spectrometry-based proteomics evidences. *Nucleic Acids Res.* **50**, D543–D552 (2022).

Acknowledgements

We thank Melissa Leyden for preparing MS figures and Emily Zahn and Ellen Speers for conducting the MS analyses. We also thank Neil Olszewski for providing plasmids JO15 and JO35. This work was supported by the National Institutes of Health (GM100051 and GM150029 to T.P.S., and GM037537 to D.F.H.), the National Science Foundation (MCB-1818161 and MCB-2416564 to T.P.S.), and the Hargitt Fellowship to X.H.

Author contributions

T.-p.S., R.Z. and J.P. conceived and designed the research project. X.H., R.Z. and J.P. performed molecular biology, genetics and biochemical analyses, and X.H., J.P., R.Z. and T.-p.S. analyzed the data and generated figures. L.R., D.L.B., M.M.R., J.S. and D.F.H. analyzed the MS/MS data. T.-p.S. and X.H. wrote the manuscript with input from all co-authors.

Competing interests

The authors declare no competing interests.

Additional information

Supplementary information The online version contains supplementary material available at https://doi.org/10.1038/s41467-024-52033-x.

Correspondence and requests for materials should be addressed to Tai-ping Sun.

Peer review information *Nature Communications* thanks Xingliang Hou, and the other, anonymous, reviewer(s) for their contribution to the peer review of this work. A peer review file is available.

Reprints and permissions information is available at http://www.nature.com/reprints

Publisher's note Springer Nature remains neutral with regard to jurisdictional claims in published maps and institutional affiliations.

Open Access This article is licensed under a Creative Commons Attribution-NonCommercial-NoDerivatives 4.0 International License, which permits any non-commercial use, sharing, distribution and reproduction in any medium or format, as long as you give appropriate credit to the original author(s) and the source, provide a link to the Creative Commons licence, and indicate if you modified the licensed material. You do not have permission under this licence to share adapted material derived from this article or parts of it. The images or other third party material in this article are included in the article's Creative Commons licence, unless indicated otherwise in a credit line to the material. If material is not included in the article's Creative Commons licence and your intended use is not permitted by statutory regulation or exceeds the permitted use, you will need to obtain permission directly from the copyright holder. To view a copy of this licence, visit http://creativecommons.org/licenses/by-nc-nd/4.0/.

© The Author(s) 2024